

Ideal Two-Fluid Simulations of Collisionless Reconnection and the Z-Pinch using the Discontinuous Galerkin Method

John Loverich and Uri Shumlak

University of Washington

Department of Aeronautics and Astronautics

IEEE International Conference on Plasma Science

Monterey, California, June 18-23, 2005

URL <http://www.aa.washington.edu/cfdlab>

email: jlovric@u.washington.edu

Abstract

A multi-dimensional algorithm using the discontinuous Galerkin method is developed for the two-fluid plasma model. The algorithm is tested on the GEM challenge magnetic reconnection problem for which it produces results in agreement with published solutions. An axisymmetric version of the code is then used to investigate axisymmetric instabilities in a Z-pinch for which a fast instability attributed to ion diamagnetic drift develops when the pinch radius is of the order of the ion Larmor radius.

Introduction

Numerical methods for several fluid plasma models have been studied extensively, especially MHD and Hall MHD. The purpose of this work is to develop an algorithm for the complete two-fluid plasma model, a model for which there is little published numerical work. Simulation of plasma phenomena using the full two-fluid plasma model allows for the analysis of effects such as charge separation and electron inertia which require a two-fluid description as well phenomena that can be described by the simpler Hall MHD model, such as the Hall effect and diamagnetic drift.

Two-Fluid Model: Maxwell's Equations

The two-fluid plasma model consists of a set of fluid equations for the electrons and ions plus the complete Maxwell's equations including displacement current,

$$\partial_t \bar{E} - c^2 (\nabla \times \bar{B}) = -\frac{1}{\epsilon_0} \sum_s \frac{q_s}{m_s} \rho_s \bar{U}_s, \quad (1)$$

$$\partial_t \bar{B} + (\nabla \times \bar{E}) = 0. \quad (2)$$

$$\nabla \cdot \bar{B} = 0 \quad (3)$$

$$\nabla \cdot \bar{E} = \frac{1}{\epsilon_0} (q_i n_i + q_e n_e) \quad (4)$$

Equations (3) and (4) are constraint equations which can be derived from Ampere's law (1) and Faraday's law (2). Equations (3) and (4) are not solved numerically, but they should be watched carefully as errors in these equations can cause serious problems[4].

Two-Fluid Model: Fluid Equations

Electrons and ions have separate energy,

$$\partial_t e_s + \nabla \cdot (\bar{U}_s (e_s + P_s)) = \frac{q_s}{m_s} \rho_s \bar{E} \cdot \bar{U}_s ,$$

momentum,

$$\partial_t \rho_s \bar{U}_s + \nabla_\alpha (\rho_s \bar{U}_s^\alpha \bar{U}_s) + \nabla_\alpha (\delta^{\alpha\beta} P_s) = \frac{q_s}{m_s} \rho_s (\bar{E} + \bar{U}_s \times \bar{B}) ,$$

and continuity,

$$\partial_t \rho_s + \nabla \cdot (\rho_s \bar{U}_s) = 0 .$$

so each species has its own temperature, velocity and number density. As a result, quasi-neutrality is not assumed and things like electron plasma waves double layers, and ion current should be observed numerically.

Two-Fluid Model: Balance Form

This set of equations can be written as three systems of balance laws,

$$\frac{\partial Q_e}{\partial t} + \nabla \cdot F_e(Q) = \psi_e, \quad (5)$$

for the electron fluid equations,

$$\frac{\partial Q_i}{\partial t} + \nabla \cdot F_i(Q) = \psi_i, \quad (6)$$

for the ion fluid equations, and

$$\frac{\partial Q_{em}}{\partial t} + \nabla \cdot F_{em}(Q) = \psi_{em}, \quad (7)$$

for Maxwell's field equations.

Two-Fluid Model: Balance Form

For clarity, these balance laws Eqns.(5)-(7) are given in full form by,

$$\frac{\partial}{\partial t} \begin{pmatrix} \rho_s \\ \rho_s U_{xs} \\ \rho_s U_{ys} \\ \rho_s U_{zs} \\ e_s \end{pmatrix} + \nabla \cdot \begin{pmatrix} \rho_s U_{xs} & \rho_s U_{ys} & \rho_s U_{zs} \\ \rho_s U_{xs} U_{xs} + P_s & \rho_s U_{xs} U_{ys} & \rho_s U_{xs} U_{zs} \\ \rho_s U_{ys} U_{xs} & \rho_s U_{ys} U_{ys} + P_s & \rho_s U_{ys} U_{zs} \\ \rho_s U_{zs} U_{xs} & \rho_s U_{zs} U_{ys} & \rho_s U_{zs} U_{zs} + P_s \\ U_{xs} (e_s + P_s) & U_{ys} (e_s + P_s) & U_{zs} (e_s + P_s) \end{pmatrix} = \begin{pmatrix} 0 \\ q_s n_s (E_x + U_{ys} B_z - U_{zs} B_y) \\ q_s n_s (E_y + U_{zs} B_x - U_{xs} B_z) \\ q_s n_s (E_z + U_{xs} B_y - U_{ys} B_x) \\ q_s n_s (E_x U_{xs} + E_y U_{ys} + E_z U_{zs}) \end{pmatrix}$$

$$\frac{\partial}{\partial t} \begin{pmatrix} B_x \\ B_y \\ B_z \\ E_x \\ E_y \\ E_z \end{pmatrix} + \nabla \cdot \begin{pmatrix} 0 & E_z & -E_y \\ -E_z & 0 & E_x \\ E_y & -E_x & 0 \\ 0 & -c^2 B_z & c^2 B_y \\ c^2 B_z & 0 & -c^2 B_x \\ -c^2 B_y & c^2 B_x & 0 \end{pmatrix} = \begin{pmatrix} 0 \\ 0 \\ 0 \\ -\frac{1}{\epsilon_0} (q_e n_e U_{xe} + q_i n_i U_{xi}) \\ -\frac{1}{\epsilon_0} (q_e n_e U_{ye} + q_i n_i U_{yi}) \\ -\frac{1}{\epsilon_0} (q_e n_e U_{ze} + q_i n_i U_{zi}) \end{pmatrix}$$

Discontinuous Galerkin Method

Discontinuous Galerkin methods are high order extensions of upwind schemes using a finite element formulation where the elements are discontinuous at cell interfaces. Details of the method are discussed in [3] and reproduced here for our particular case. The balance law,

$$\frac{\partial Q}{\partial t} + \nabla \cdot F = \psi ,$$

is multiplied by the set of basis functions $\{v_r\}$ and integrated over the finite volume element K . For second order spatial accuracy the basis set $\{v_r\} = \{v_0, v_x, v_y\} = \{1, \frac{x-x_{ij}}{\frac{1}{2}\Delta x}, \frac{y-y_{ij}}{\frac{1}{2}\Delta y}\}$ is used. The equation is written,

$$\int \frac{\partial Q}{\partial t} v_r dV + \int (\nabla \cdot F) v_r dV = \int \psi v_r dV .$$

Discontinuous Galerkin Method

Integrate by parts to get

$$\int_K \frac{\partial Q}{\partial t} v_r dV + \int_{\partial K} (F \cdot n) v_r d\Gamma - \int_K F \cdot (\nabla v_r) dV = \int_K \psi v_r dV .$$

The discrete conserved variable Q is defined as a linear combination of the basis

functions inside an element K , $Q = Q_0 + v_x Q_x + v_y Q_y$. The integral

$\int_K \frac{\partial Q}{\partial t} v_r dV = \frac{\partial Q_r}{\partial t} C V$ where C is the constant $\frac{1}{V} \int_K v_r^2 dV$ and V is the volume of the element. Using these definitions we get the discrete equation

$$\frac{\partial Q_r}{\partial t} C V + \sum_e \sum_l r_l (F \cdot n) v_r \Gamma_e - \sum_m w_m F \cdot (\nabla v_r) V = \sum_m w_m \psi v_r V ,$$

when the integrals are replaced by appropriate Gaussian quadratures. Γ_e is the surface area of the cell face in consideration, e refers to an element face, r_l are quadrature points on a face and w_m are quadrature points in the volume.

Discontinuous Galerkin Method

The discrete equations for the second order scheme are

$$\frac{\partial Q_0}{\partial t} V + \sum_e \sum_l r_l (F \cdot n) v_0 \Gamma_e = \sum_m w_m \psi v_0 V ,$$

$$\frac{\partial Q_x}{\partial t} V + 3 \sum_e \sum_l r_l (F \cdot n) v_x \Gamma_e - 3 \sum_m w_m F \cdot (\nabla v_x) V = 3 \sum_m w_m \psi v_x V ,$$

$$\frac{\partial Q_y}{\partial t} V + 3 \sum_e \sum_l r_l (F \cdot n) v_y \Gamma_e - 3 \sum_m w_m F \cdot (\nabla v_y) V = 3 \sum_m w_m \psi v_y V .$$

The derivatives of the basis functions can be calculated analytically since the polynomial basis functions are known. The discontinuous Galerkin method is applied to each balance law (5)(6)(7) at every time step. In [2] TVD Runge-Kutta time integration is suggested, though standard Runge-Kutta methods work well. In this paper we use a 3rd order TVD Runge-Kutta scheme as in [2].

Magnetic Reconnection: GEM Challenge

In ideal MHD the fluid is frozen to the magnetic field lines and so field lines cannot reconnect without some non-ideal term. Resistivity allows field lines to reconnect though much slower than the fast reconnection that occurs in collisionless space and fusion plasmas. This fast reconnection requires at least the addition of the Hall term, but the heuristic approach to electron dissipation can be avoided if electron inertia is included - this requires a two-fluid solution.

The GEM challenge magnetic reconnection problem is non-dimensionalized as in [1] where lengths are normalized by the ion inertial length $d = c/w_{pi} = c \left(\frac{e^2 n_0}{\epsilon_0 m_i} \right)^{-\frac{1}{2}}$ time is non-dimensionalized by the ion-cyclotron time $\frac{m_i}{e B_0}$ where B_0 is the magnetic field at infinity. The domain is $[-\frac{1}{2}L_x d, \frac{1}{2}L_x d] \times [-\frac{1}{2}L_y d, \frac{1}{2}L_y d]$ with $L_x = 25.6$ and $L_y = 12.8$. Conducting boundary conditions are used on the y boundaries while periodic boundary conditions are used on the x boundaries. In this simulation $\lambda = 0.5 d$ and the ion to electron mass ratio is taken to be 25, the specific heat ratio $\gamma = \frac{5}{3}$ for both electrons and ions and $\frac{V_a}{c} = \frac{1}{10}$.

Magnetic Reconnection: GEM Challenge

The initial number densities are given by,

$$n_e = n_i = n_0 \left(\frac{1}{5} + \operatorname{sech}^2 \left(\frac{y}{\lambda} \right) \right) .$$

The electron pressure is $P_e = \frac{1}{12\mu_0} B_0^2 \frac{n_e}{n_0}$ and the ion pressure is $P_i = \frac{5}{12\mu_0} B_0^2 \frac{n_i}{n_0}$. The magnetic field is given by

$$B_x = B_0 \tanh \left(\frac{y}{\lambda} \right) + \frac{B_0}{10} \frac{\pi}{L_x} \cos \left(\frac{2\pi x}{L_x} \right) \sin \left(\frac{\pi y}{L_y} \right)$$

$$B_y = \frac{B_0}{10} \left(\frac{2\pi}{L_x} \right) \sin \left(\frac{2\pi x}{L_x} \right) \cos \left(\frac{\pi y}{L_y} \right)$$

The initial electron current J_{ze} is,

$$J_{ze} = -\frac{\mu_0 B_0}{\lambda} \operatorname{sech}^2 \left(\frac{y}{\lambda} \right) .$$

Magnetic Reconnection: In Plane Current

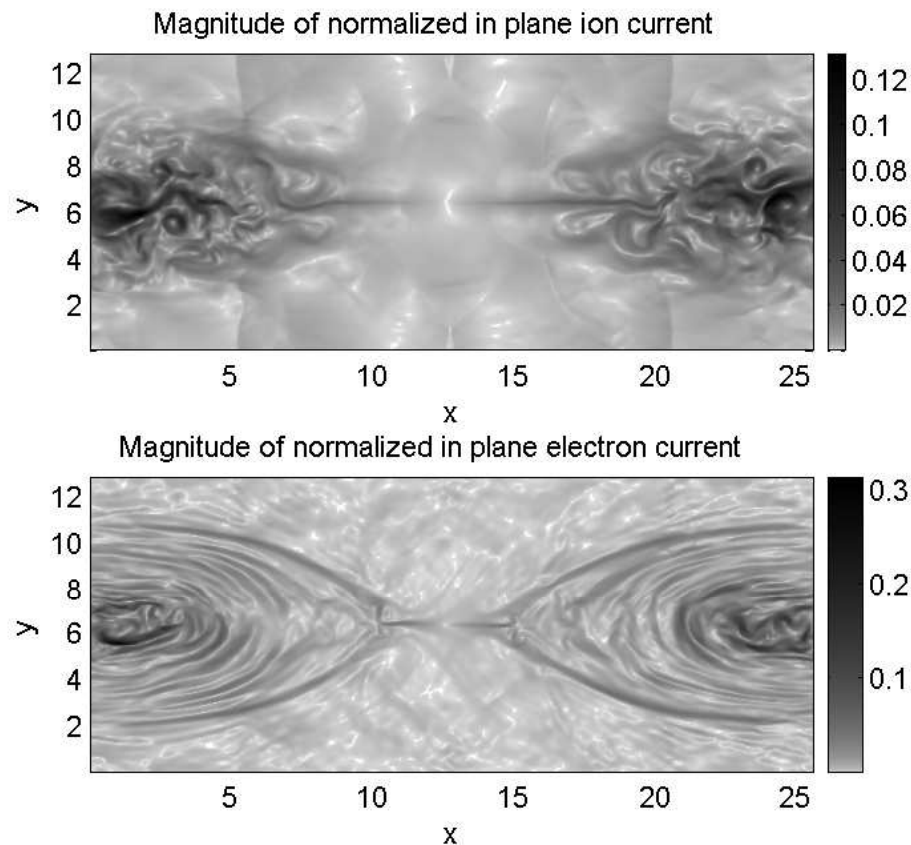


Figure 1: Magnitude of in plane current in the GEM challenge problem after $t = 40/\omega_{ci}$. The electron and ion currents differ substantially in structure because the electrons are frozen to the field lines over a greater range than the ions.

Magnetic Reconnection: Out Of Plane Current

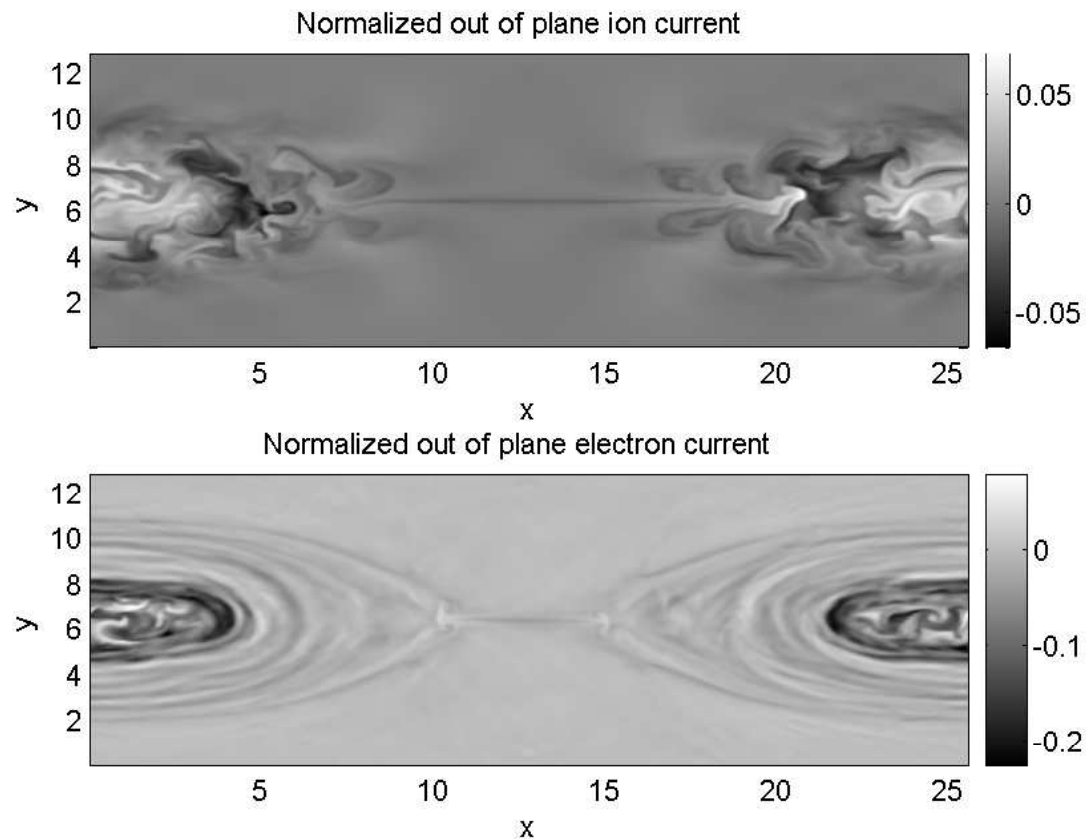


Figure 2: Out of plane current in the GEM challenge problem after $t = 40/\omega_{ci}$. The initial electron current is out of plane, this current collects in the lobes late in time. The ions contribute little to the out of plane current.

Magnetic Reconnection: Species Number Density

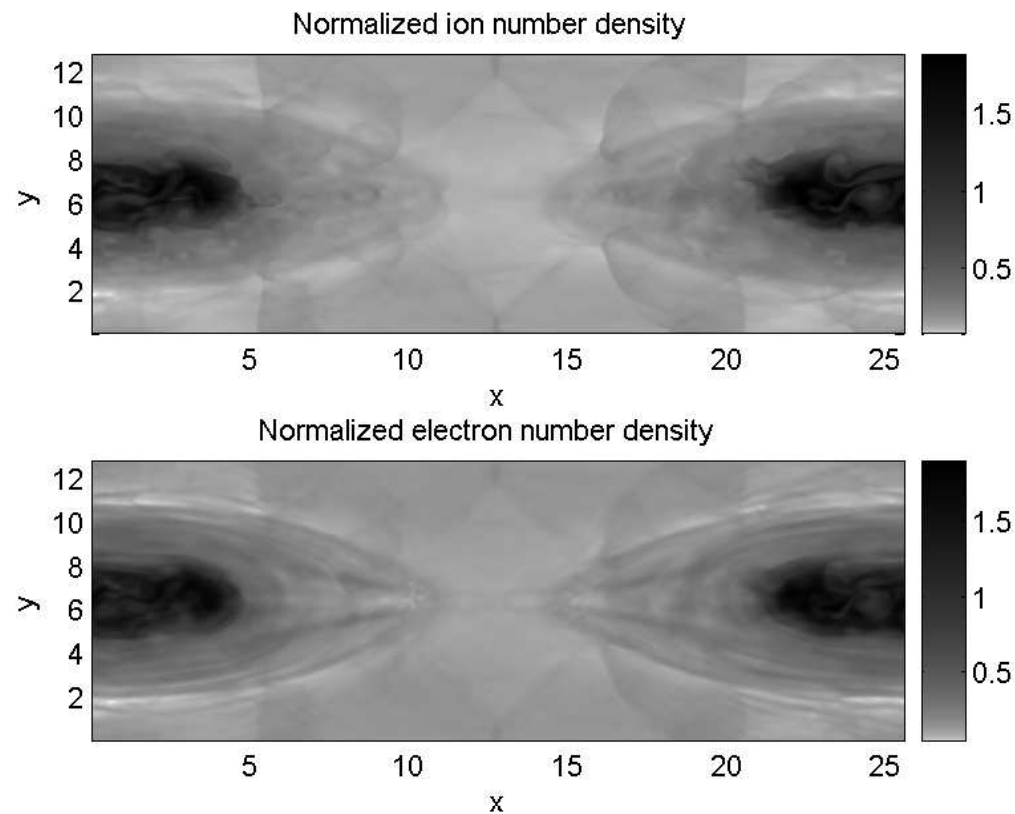


Figure 3: Number density in the GEM challenge problem after $t = 40/\omega_{ci}$. A number of ion shocks are evident in this plot. The electrons don't shock, so the electrons show smoother transitions where the ions show sharp discontinuities

Magnetic Reconnection: Magnitude of in Plane Electric Field

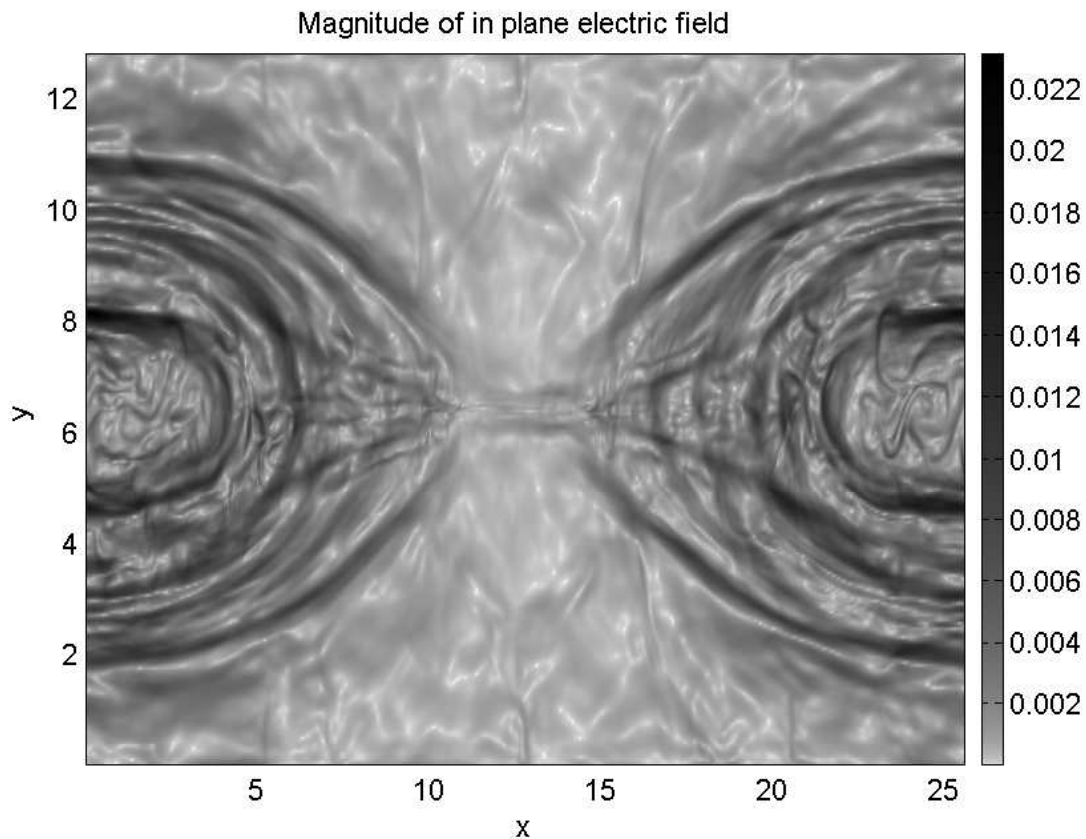


Figure 4: Magnitude of in plane electric field. These electric fields are mainly due to charge separation. The electron inertial length is resolved in these simulations so some of the in plane field will be due to purely electromagnetic waves, particularly in the low density regions.

Magnetic Reconnection

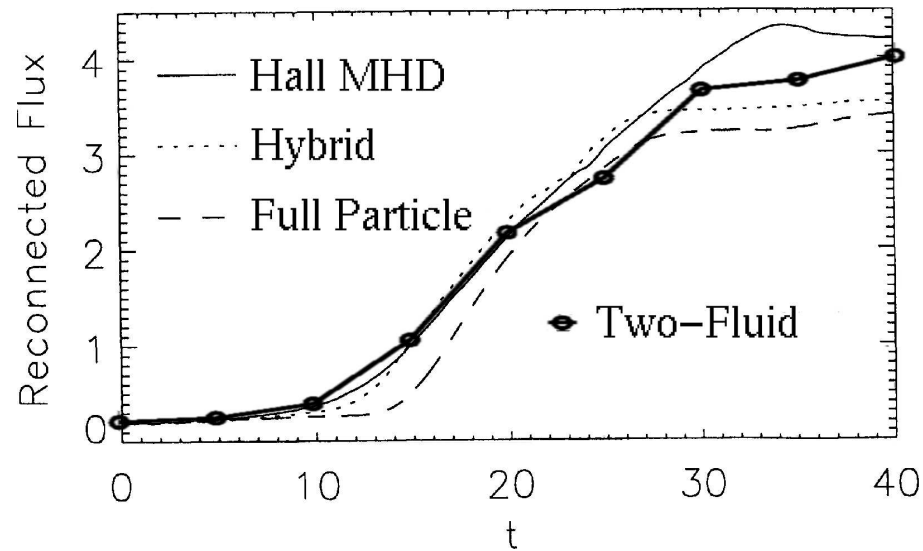


Figure 5: Plot taken from [5] with the two-fluid solution calculated by the authors superimposed on top. Plot of reconnected magnetic flux vs time in units of inverse ω_{ci} for several published solutions and the two-fluid solution calculated by the authors.

Magnetic Reconnection

Using the full two-fluid system allows for completely separate electron and ion dynamics, which can be seen in Fig. 1. The use of a shock capturing scheme allows the resolution of many different shocks in Fig. 3. Also, since electrons and ions may have different densities, the electric field is calculated from Maxwell's equations instead of using an Ohm's law, see Fig. 4. In Fig. 5 the two-fluid solution is compared to solutions published in the GEM challenge papers [1]. The two-fluid solution shows good agreement with published solutions. Differences in the two-fluid solution vs published solutions lie in the fine details, such as large scale ion turbulence and shock waves. The discontinuous Galerkin method has allowed us to resolve these fine structures.

Z-Pinch

In the following slides, an axisymmetric version of the algorithm is used to evolve axisymmetric two-fluid instabilities in the Z-Pinch. Simulations are run using 2 different pinch radii, $2.5R_{gi}$ and $12.5R_{gi}$ where R_{gi} is the ion Larmor radius. Sinusoidal perturbation in the magnetic field along the axis are used to initialize the instabilities. The solution is initialized using an MHD equilibrium with constant current carried by the electrons for $r < 0.25$. The ion to electron mass ratio is 100. The electron and ion temperatures are initially constant throughout the domain, the electron pressure equals the ion pressure and the electron number density equals the ion number density. A background density and pressure of 10% is added to prevent negative pressures.

Note: A two-fluid equilibrium differs from an MHD equilibrium so the initial conditions are only an approximate equilibrium.

Z-Pinch

Pinch radius $R = 12.5 R_{gi}$

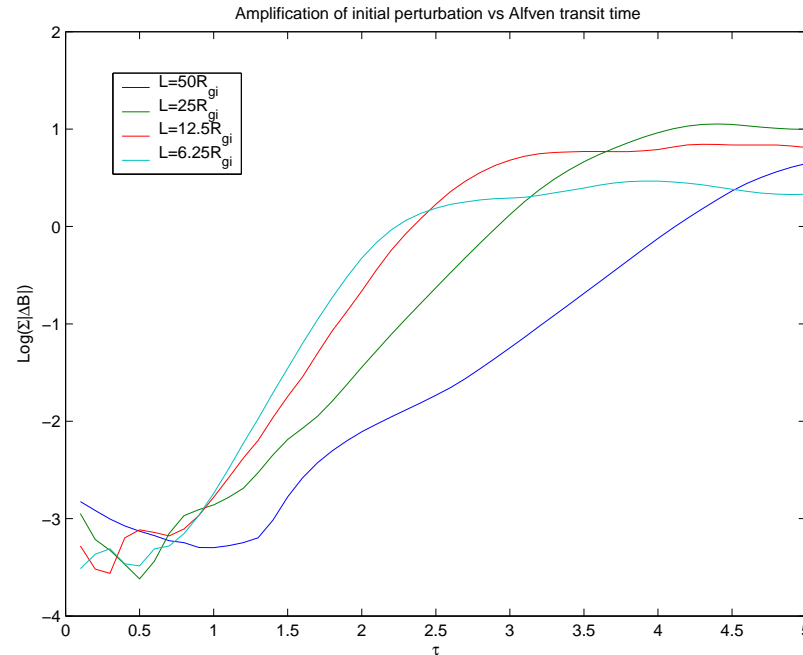


Figure 6: Plots of the growth in the perturbed magnetic field vs time normalized by the Alfvén transit time across the radius. The Z-pinch has radius $R = 12.5 R_{gi}$ and plots are shown for various wavelength perturbations L . The growth occurs on MHD time scales as expected for the sausage instability.

Z-Pinch

Pinch radius $R = 12.5 R_{gi}$, Perturbation wave length $L = 50 R_{gi}$
1 period shown

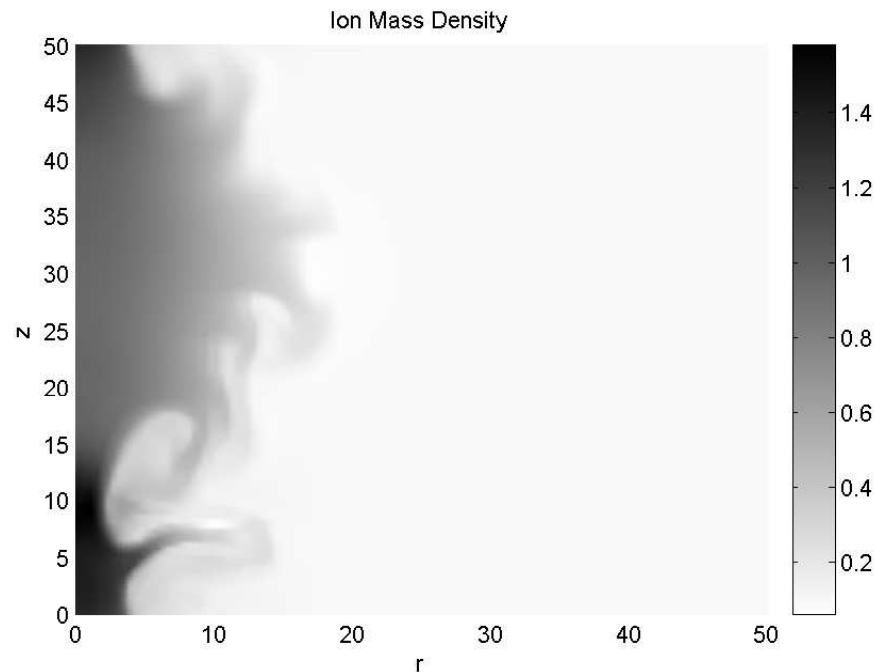


Figure 7: Ion mass density plot after $5\tau_A$. The $L = 50 R_{gi}$ perturbation grows into the non-linear regime. A higher wave number instability is nonlinearly coupled to the initial perturbation and also develops.

Z-Pinch

Pinch radius $R = 12.5 R_{gi}$, Perturbation wave length $L = 25 R_{gi}$
2 periods shown

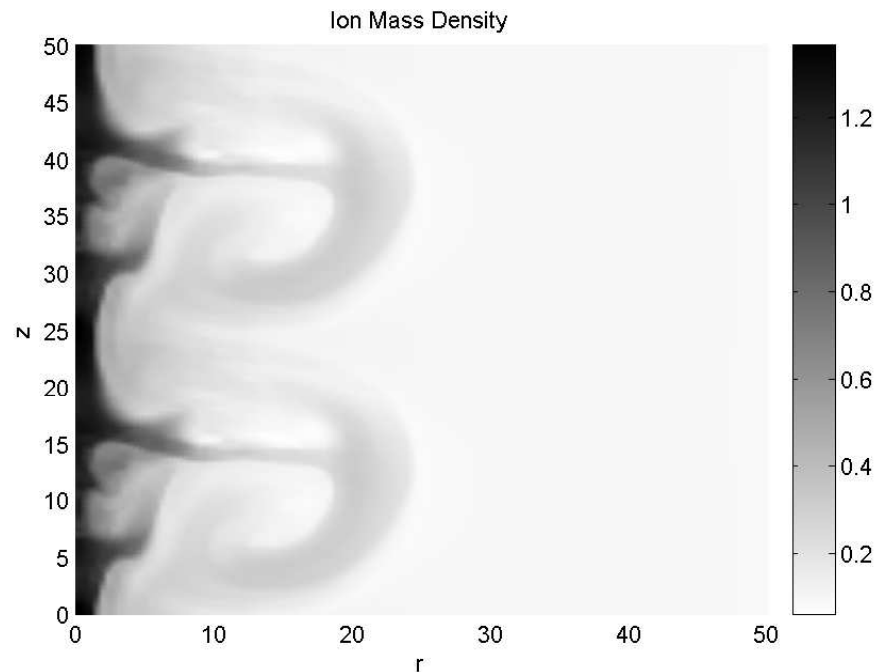


Figure 8: Ion mass density plot after $5\tau_A$. As expected, the $L = 25 R_{gi}$ perturbation grows faster than the $L = 50 R_{gi}$ perturbation - however earlier in time the $L = 25 R_{gi}$ looks very similar to the $L = 50 R_{gi}$ solution.

Z-Pinch

Pinch radius $R = 2.5 R_{gi}$

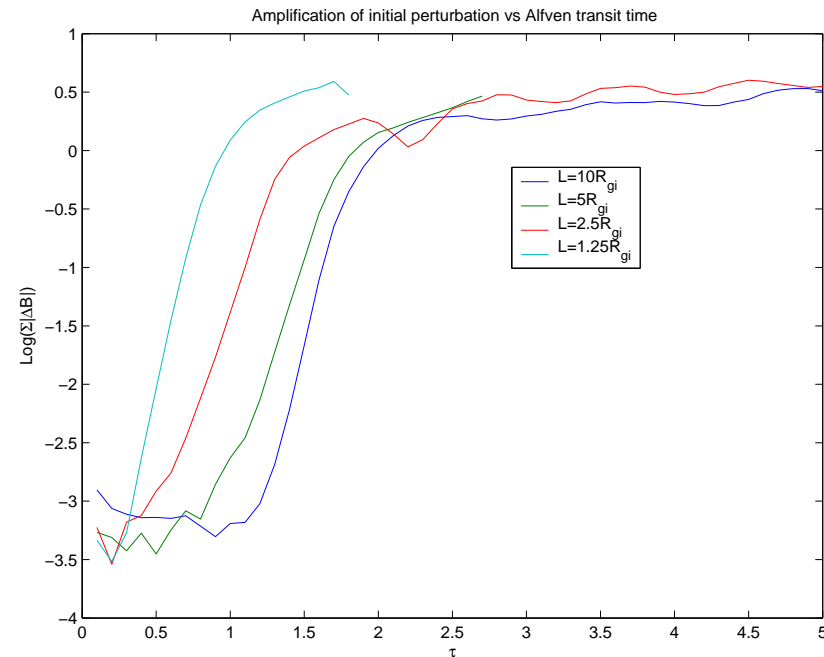


Figure 9: Plots of the growth in the perturbed magnetic field vs time normalized by the Alfvén transit time across the radius. The Z-pinch has radius $R = 2.5 R_{gi}$ and plots are shown for various wavelength perturbations L . The growth occurs faster than MHD time scales and may be associated with the ion diamagnetic drift near the edge of the pinch.

Z-Pinch

Pinch radius $R = 2.5 R_{gi}$, Perturbation wave length $L = 10 R_{gi}$
1 period shown

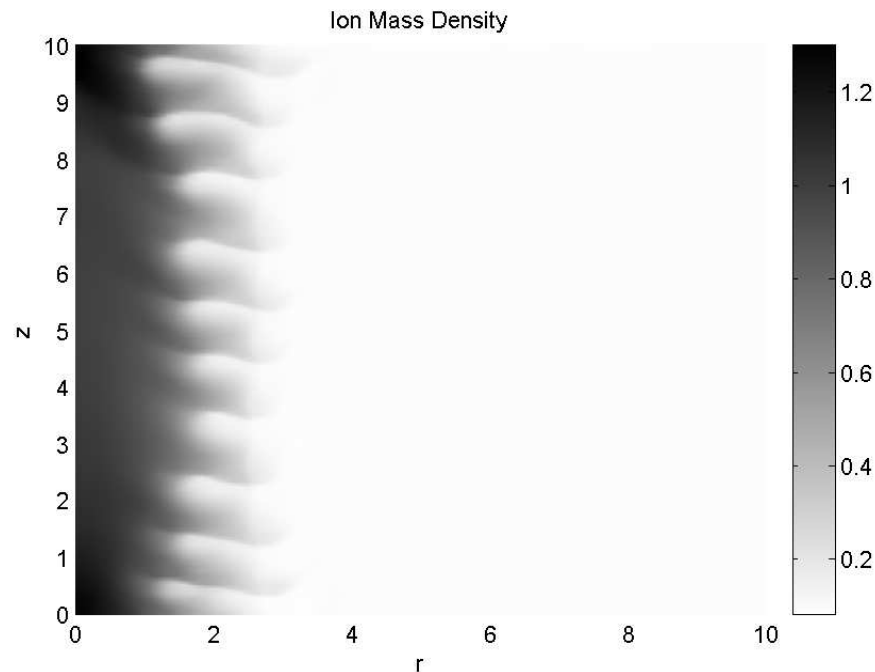


Figure 10: Ion mass density plot after $2\tau_A$. Despite the fact that the solution is initialized with an $L = 10 R_{gi}$ perturbation, waves of length $1 R_{gi}$ develop and grow faster. This short wave length mode may be related to the diamagnetic drift of the ions.

Z-Pinch

Pinch radius $R = 2.5 R_{gi}$, Perturbation wave length $L = 5 R_{gi}$
2 periods shown

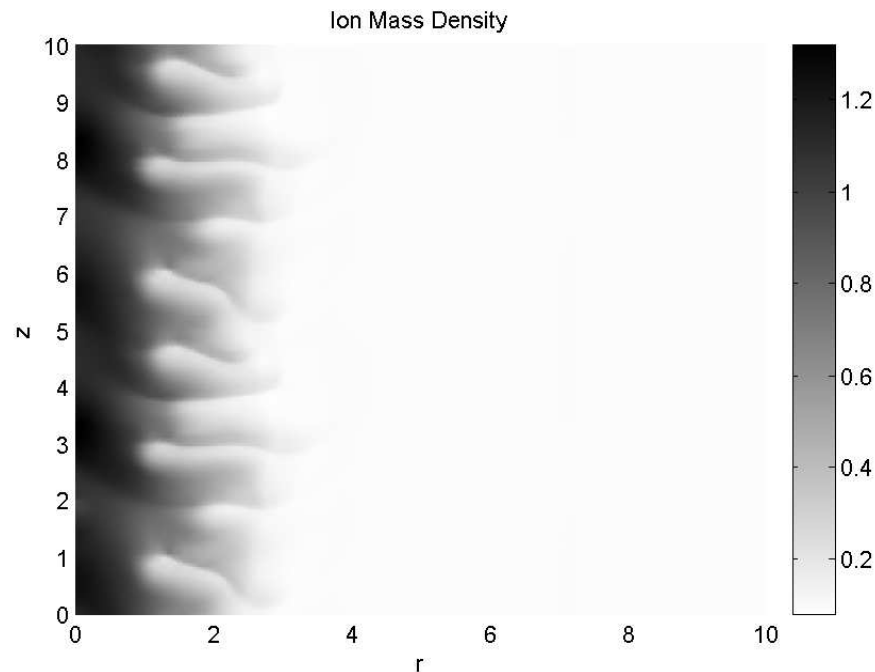


Figure 11: Ion mass density plot after $2\tau_A$. When the initial perturbation wave length is changed to $L = 5 R_{gi}$, the same short wave length $L = 1 R_{gi}$ develops and dominates the non-linear dynamics.

Z-Pinch

In cases where the radius of the pinch is significantly larger than the ion Larmor radius, the two fluid solution behaves like an MHD solution. Short wave length modes do develop, however they do not significantly change the overall dynamics. On the other hand, when the pinch radius is of the order the ion Larmor radius, a short wave length mode develops and dominates the growth, quickly penetrating to the axis before modes on MHD time scales can grow significantly. This instability may be a result of ion diamagnetic drift shear near the edge of the pinch. FLR effects, which are not included in the two-fluid model being used, should be important in this regime and may suppress this instability.

Conclusion

An algorithm for the two-fluid plasma model that uses the discontinuous Galerkin method is used to solve the GEM challenge magnetic reconnection problem for which the two-fluid solution is compared to published results. The discontinuous Galerkin method resolves shocks well and furthermore significant amounts of turbulent flow are evident late in time. An axisymmetric version of the algorithm has been used in a preliminary study of the two-fluid Z-pinch. In cases where the ion Larmor radius is small compared to the pinch radius the two-fluid solution looks similar to MHD solutions, producing sausage instabilities. When the ion Larmor radius is comparable to the pinch radius the solution differs substantially from the MHD solution, this may be a result of ion diamagnetic drift. Further investigation of the two-fluid z-pinch is required.

References

- [1] J. Birn and et al., *Geospace environmental modeling (gem) magnetic reconnection challenge*, Journal of Geophysical Research **106** (2001), no. A3, 3715–3719.
- [2] Bernardo Cockburn and Chi-Wang Shu, *Tvb runge-kutta local projection discontinuous galerkin finite element method for conservation laws ii: General framework*, Mathematics of Computation **52** (1989), 411–435.
- [3] _____, *The runge-kutta discontinuous galerkin method for conservation laws v: Multidimensional systems*, Journal of Computational Physics **141** (1998), 199–224.
- [4] Bo nan Jiang, Jie Wu, and L. A. Povinelli, *The origin of spurious solutions in computational electromagnetics*, Journal Of Computational Physics **125** (1996), 104–123.
- [5] M. A. Shay, J. F. Drake, B. N. Rogers, and R. E. Denton, *Alfvénic collisionless magnetic reconnection and the hall term*, Journal of Geophysical Research **106** (2001), 3759–3772.